

A MINDLIN SHELL FINITE ELEMENT FOR STONE MASONRY BRIDGES WITH BACKFILL

PETR ŘEŘIČHA

Czech Technical University in Prague, Faculty of Civil Engineering, Thákurova 7, Prague, Czech Republic
correspondence: petr.rericha@fsv.cvut.cz

ABSTRACT. Stone masonry bridges are difficult to analyse with commercial finite element (FE) packages for their specific heterogeneous composition. The stone arch is best modelled as a thick shell where there are predestined directions of tension failure, normal to the bed joints. A dedicated, very simple, Mindlin shell finite element is developed with five translational degrees of freedom per node. It features compatibility with linear isoparametric or constant strain elements for the backfill. Most bridges can be analysed with a sufficient accuracy assuming plain strain conditions. The element then simplifies to a Timoshenko beam element with three translational degrees of freedom per node. An application of the latter one to the bridge at Poniklá is presented.

KEYWORDS: Masonry arches, no tension joints, thick shell elements, octave script.

1. INTRODUCTION

Masonry arch bridges still constitute a considerable part of the bridge stock of the transport infrastructure in Czechia. Many of them are valuable monuments of the technical expertise and craftsmanship of the past generations as well. Design standards for this sort of bridges do not exist worldwide, guides and manuals for load rating are provided instead, like [1] or [2]. They usually contain conservative approximate methods for a routine assessment and some guidance and recommendations for more complicated individual assessments based on advanced structural analysis methods.

A structural analysis of masonry arch bridges is specific in that the ultimate limit state forces and stresses cannot be solved for assuming homogeneous isotropic linear elastic material. In contrast to that, design standards for reinforced concrete and steel structures admit such solutions. EN 1996-1-1 codifies in clause 6.1.1(2) that plane sections remain plane and the tensile strength of masonry perpendicular to bed joints is zero in the ultimate limit state. The standard is not compulsory for bridges but its conditions should be perceived as the minimum for them. Cracks in the bed joints of the masonry arches affect the stress distribution in a way that does not admit a linear solution.

The simplest material model that can be accepted is the no-tension linear material where the no-tension condition applies to the normal stress in the planes parallel to the bed joints. This specific behaviour is difficult to simulate by material models available in general purpose program packages, [3]. Commercial packages do not include such material models. There were attempts to achieve the specific properties of the masonry arches with a trivial model of a heterogeneous material – individual meshing of voussoirs and joints by standard continuum finite elements

with homogeneous material models. It is possible in academic works but not acceptable in design practice for demands on the labour, software and input data on materials properties. This experience testifies that *shell/beam elements using the rigid normals assumption (Timoshenko, Mindlin, Bernoulli-Navier and other assumptions) are indispensable for the solution of the masonry arch bridges.*

Several dedicated codes have been written around 1990 for the analysis of masonry arches based on the Castigliano principle, CTAP [4], [5], rigid block assumption RING, [6], mechanism based ARCHIE, [7] and others. All of them assume plane strain conditions. These models simulate very well the observed behaviour of masonry arches in situ and in large scale model tests. They have been applied worldwide in practice despite their common drawback that they underestimate the interaction of the barrel, backfill and pavement.

Two simple finite elements for thick shells are developed based on the Timoshenko/Mindlin kinematic assumptions, one for plane stress/plane strain conditions, the other for 3D shells. In order to facilitate a seamless interaction with the backfill continuum, only translational degrees of freedom (DOFs) are employed. The no-tension linear elastic constitutive equations are integrated in a closed form for the normal stress in planes parallel to the bed joints. The shape functions of the elements are 2D and 3D variants of the same concept. The simpler 2D variant is presented first with an application to a bridge, a triangle thick shell element follows.

2. THE TT ELEMENT, TIMOSHENKO BEAM WITH TRANSLATIONAL DOFS

The displacement shape functions are sketched in Figure 1 for the axial displacement $u_{i,t}$ of node i , for the

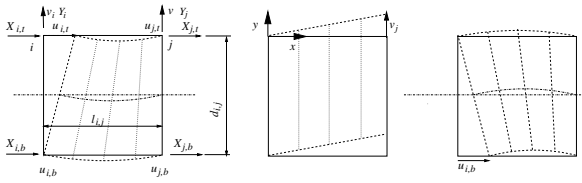


FIGURE 1. Shape functions, DOFs and conjugate nodal forces of the TT element

lateral displacement v_j of node j and for the axial displacement $u_{i,b}$. Axial and lateral directions denote the element local x and y directions, indices t and b denote the top and bottom faces later also extrados and intrados of the arch. The local x axis goes from node i to node j . The deflection line is parabolic and symmetric. It's single free parameter is determined so that the shear strain energy is minimum for any imposed node displacements. Analogous shape functions are valid for all four axial DOFs $u_{i/j,t/b}$ and the same applies to the two lateral DOFs $v_{i/j}$.

The cross-sections remain straight but not normal to the deflected beam axis. In an isoparametric beam element (linear variation of the cross-section rotations and shear deformation, axial strain and lateral deflections along the beam axis), there would be no deflections for the $u_{i/j,t}$ DOFs. The element is known to lock for small depths of the beam owing to excessive work of the shear deformation. The present element features a constant shear deformation since the anti-symmetric (with respect to the element centre) part of the cross-section rotations is assigned to a constant curvature of the deflection line. The element DOFs are ordered in the $\{u\}$ matrix,

$$\{u\} = \left\{ \begin{matrix} \{u\}_i \\ \{u\}_j \end{matrix} \right\}, \quad \{u\}_n = \left\{ \begin{matrix} u_{n,t} \\ v_n \\ u_{n,b} \end{matrix} \right\}, \quad n = i, j$$

Linear normal and constant shear element strains are specified by top and bottom face normal strains $\varepsilon_t, \varepsilon_b$ and shear strain γ , ordered in the matrix of internal strains $\varepsilon = \{\varepsilon_t, \varepsilon_b, \gamma\}^T$. Shear strain γ and conjugate shear stress τ have opposite signs than usual in elasticity, $\gamma = -(\partial u_x / \partial y + \partial u_y / \partial x) / 2$. The element geometric matrix $[B]$ reads:

$$[B] = \frac{1}{l} \begin{bmatrix} -1 & 0 & 0 & 1 & 0 & 0 \\ 0 & 0 & -1 & 0 & 0 & 1 \\ l/2/d & -1 & -l/2/d & l/2/d & 1 & -l/2/d \end{bmatrix}$$

Conjugate to node displacements $\{u\}$ are the nodal forces $\{X\}$, conjugate to $\{\varepsilon\}$ is the matrix of internal forces $\{S\}$. The nodal forces in terms of nodal displacements read

$$\{X\} = [B]^T \{S\} (\{\varepsilon\}) = [B]^T \{S\} ([B] \{u\}) \quad (1)$$

Constitutive equations for the cross-section are developed separately for the bending, the first two members of $\{\varepsilon\}$ and $\{S\}_{int}$.

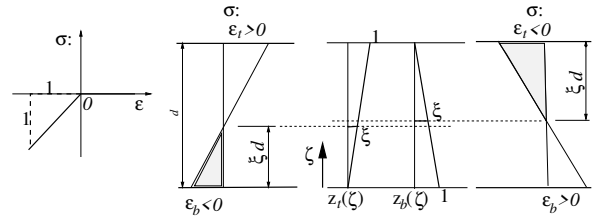


FIGURE 2. Stress/strain diagram, strain shape functions and normal stress diagrams of the TT element

2.1. CONSTITUTIVE EQUATIONS FOR BENDING

No-tension linear elastic material is assumed, see the stress-strain diagram in Figure 2. The no-tension condition is applied to the normal stress in cross-sections and bed joints of the arch. Though simple, it makes possible the most frequent type of failure of the stone masonry arch bridges. The normal strain ε is determined by the top and bottom face strains $\varepsilon_t, \varepsilon_b$ through the shape functions shown in the centre of Figure 2.

$$\varepsilon = z_t(\zeta)\varepsilon_t + z_b(\zeta)\varepsilon_b$$

Constitutive equations of the cross-sections are defined in terms of dimensionless functions $s_t()$ and $s_b()$ of dimensionless arguments:

$$\begin{aligned} s_t(\varepsilon_t, \varepsilon_b) &= \int_0^1 z_t(\zeta) s(\varepsilon_t z_t(\zeta) + \varepsilon_b z_b(\zeta)) d\zeta \\ s_b(\varepsilon_t, \varepsilon_b) &= \int_0^1 z_b(\zeta) s(\varepsilon_t z_t(\zeta) + \varepsilon_b z_b(\zeta)) d\zeta, \quad (2) \end{aligned}$$

The cross-section forces are $S_{t/b} = Ebd s_{t/b} = EAs_{t/b}$ (valid for both t and b subscripts, where E is the Young modulus, b the cross-section width, d the cross-section depth and A its area. Functions $s_{t/b}()$ and their derivatives with respect to $\varepsilon_t, \varepsilon_b$ have to be developed separately for four possible strain states:

Algorithm start

When $\varepsilon_t > 0$ and $\varepsilon_b > 0$ then all internal forces are 0, the cross-section is totally disintegrated. All stresses and internal forces vanish in the element.

When $\varepsilon_t > 0$ and $\varepsilon_b < 0$, then (see the left strain diagram in Figure 2):

$$\xi = \frac{\varepsilon_b}{\varepsilon_b - \varepsilon_t}$$

$$s_t = \varepsilon_b \xi^2 / 6, \quad s_b = (0.5 - \xi / 6) \xi \varepsilon_b$$

$$\frac{\partial s_t}{\partial \varepsilon_t} = \xi^3 / 3, \quad \frac{\partial s_t}{\partial \varepsilon_b} = \left(1 - 2\xi \frac{\varepsilon_t}{\varepsilon_b}\right) \frac{\xi^2}{6}$$

$$\frac{\partial s_b}{\partial \varepsilon_t} = (0.5 - \xi / 3) \xi^2, \quad \frac{\partial s_b}{\partial \varepsilon_b} = (0.5 - \frac{\xi}{6}) \xi - (0.5 - \frac{\xi}{3}) \xi^2 \frac{\varepsilon_t}{\varepsilon_b}$$

When $\varepsilon_t < 0$ and $\varepsilon_b > 0$, then (see the right strain diagram in Figure 2):

$$\xi = \frac{\varepsilon_t}{\varepsilon_t - \varepsilon_b}$$

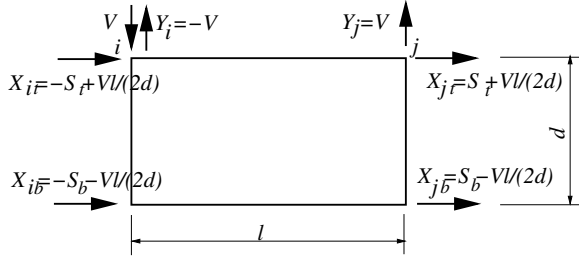


FIGURE 3. Element internal forces $\{S\}$ and nodal forces $\{X\}$

$$s_t = (0.5 - \frac{\xi}{6})\xi\varepsilon_t, \quad s_b = \varepsilon_t\xi^2/6$$

$$\frac{\partial s_t}{\partial \varepsilon_t} = (0.5 - \frac{\xi}{6})\xi - (0.5 - \frac{\xi}{3})\xi^2 \frac{\varepsilon_b}{\varepsilon_t}, \quad \frac{\partial s_t}{\partial \varepsilon_b} = (0.5 - \xi/3)\xi^2$$

$$\frac{\partial s_b}{\partial \varepsilon_t} = \left(1 - 2\xi \frac{\varepsilon_b}{\varepsilon_t}\right) \frac{\xi^2}{6}, \quad \frac{\partial s_b}{\partial \varepsilon_b} = \xi^3/3$$

When $\varepsilon_t < 0$ and $\varepsilon_b < 0$, then the cross-section is linear elastic and dimensionless generalised forces are

$$s_{t/b} = (2\varepsilon_{t/b} + \varepsilon_{b/t})/6$$

The cross-section stiffness matrix:

$$\frac{\partial \{s_{bend}\}}{\partial \{\varepsilon_{bend}\}} = \frac{1}{6} \begin{bmatrix} 2 & 1 \\ 1 & 2 \end{bmatrix} \quad (3)$$

Algorithm end

The bending stiffness tangent matrix of the cross-section is denoted for a later reference

$$[D_{bend}] = \frac{\partial \{s_{bend}\}}{\partial \{\varepsilon_{bend}\}} = Ebd \begin{bmatrix} \frac{\partial s_t}{\partial \varepsilon_t} & \frac{\partial s_t}{\partial \varepsilon_b} \\ \frac{\partial s_b}{\partial \varepsilon_t} & \frac{\partial s_b}{\partial \varepsilon_b} \end{bmatrix} \quad (4)$$

2.2. FULL CROSS-SECTION STIFFNESS MATRIX

The shear force V is computed from the shear deformation γ in the Timoshenko beam. Linear elastic behaviour

$$V = G_ebd\gamma$$

is assumed in the model, independent on the normal stress in the cross-sections. This assumption is mostly sufficient for cross-sections of the stone masonry arch bridges. The full cross-section stiffness matrix is then

$$[D_{cs}] = \begin{bmatrix} [D_{bend}] & \{0\} \\ \{0\}^T & G_ebd \end{bmatrix}$$

The matrix has to be adapted when more involved cross-section constitutive equations are necessary, for instance, shear failure of bed joints. The nodal forces $\{X\} = \{X_{i,t}, Y_i, X_{i,b}, X_{j,t}, Y_j, X_{j,b}\}^T$ of the element can be obtained in terms of the internal forces $\{S\}$ either by expansion of $[B]^T\{S\}$ or by the equilibrium conditions of the element in Figure 3: The dimensionless cross-section stiffness matrix for bending $[D_{bend}] = \partial\{S_{bend}\}/\partial\{\varepsilon_{bend}\}$ is not symmetric when the neutral axis lies inside the cross-section so that the

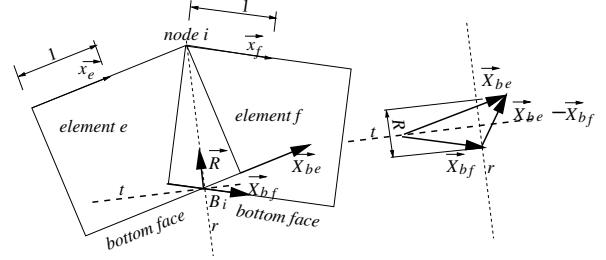


FIGURE 4. Equilibrium of node i

element and structure matrices will not be symmetric, too. The element stiffness matrix is

$$[K]_{straight} = Ebdl[B]^T[D_{cs}][B]$$

It is ready for application in straight beams, but for arches and other curved beams, it must be modified.

2.3. ARCH NODES EQUILIBRIUM

The equilibrium of the nodal forces $\vec{X}_{ibe} = X_{ibe}\vec{x}_e$, $\vec{X}_{ibf} = X_{ibf}\vec{x}_f$ of the adjacent elements e and f at arch node i simplifies to $X_{ibe} + X_{ibf} = 0$ when the element's unit length direction vectors $\vec{x}_{l,e}$ and $\vec{x}_{l,f}$ coincide, see the Figure 4. The node index i is omitted for brevity as long as the the development concerns just a single node i . X_{be} and X_{bf} are the magnitudes of the respective forces with positive senses in element's direction vectors. These forces are stored in the third components of the element nodal forces matrices and in case of parallel elements, the equilibrium equation at a node is $\{X\}_e + \{X\}_f = \{0\}$, where indices e and f indicate the left and right element, respectively.

When the adjacent elements are not parallel, the resultants of the two forces add up to force \vec{R} . The force is decomposed into component R in the direction r and force T in the t direction. The component R can act anywhere on ray r since the arch is considered rigid in the transverse direction. It is thus added to forces acting at node i . Component T must vanish to keep the null moment with respect to joint i .

$$T = (X_{be}\vec{x}_e + X_{bf}\vec{x}_f) \cdot \vec{t} = (X_{be}\vec{x}_e + X_{bf}\vec{x}_f) \cdot (\vec{x}_e + \vec{x}_f) / |\vec{x}_e + \vec{x}_f| = 0,$$

which implies

$$X_{be} + X_{bf} = 0,$$

provided the two elements are not normal to each other. Force R is

$$R = (X_{be}\vec{x}_e - X_{bf}\vec{x}_f) \cdot \vec{r} = (X_{be}\vec{x}_e - X_{bf}\vec{x}_f) \cdot (\vec{x}_e - \vec{x}_f) / |\vec{x}_e - \vec{x}_f| = (X_{be} - X_{bf})\sqrt{(1 - \vec{x}_e \cdot \vec{x}_f)}/2$$

and its vector

$$\vec{R} = R\vec{r} = 0.5(X_{be} - X_{bf})(\vec{x}_e - \vec{x}_f)$$

The ray r of the force must connect points i and B_i , the intersection of the \vec{X}_{be} and \vec{X}_{bf} forces rays, otherwise node i would not be in equilibrium. Ray r is approximately radial to the arch. Vector

$$\vec{g} = 0.5(\vec{x}_e - \vec{x}_f) \quad (5)$$

is an important property of node i . The matrix expression for vector \vec{R} is in terms of \vec{g}

$$\vec{R} = \{\vec{g}, -\vec{g}\} \begin{Bmatrix} X_{be} \\ X_{bf} \end{Bmatrix}$$

Recall that X_{be} denotes the third element of the nodal forces matrix of element e at node i and the analogue holds for X_{bf} . Conjugate displacements to X_{be} and X_{bf} are u_{be} and u_{bf} , conjugate to \vec{R} is the displacement vector \vec{u} of node i . The principle of virtual work thus implies

$$\begin{Bmatrix} u_{be} \\ u_{bf} \end{Bmatrix} = \begin{Bmatrix} \vec{g} \\ -\vec{g} \end{Bmatrix} \cdot \vec{u}$$

The same result can be obtained when the part of \vec{u} in \vec{r} direction, $(\vec{u} \cdot \vec{r})\vec{r}$, is projected on the \vec{x}_e direction to obtain u_{be} :

$$u_{be} = (\vec{u} \cdot \vec{r})\vec{r} \cdot \vec{x}_e = \vec{g} \cdot \vec{u}.$$

Projection on \vec{x}_e yields the same expression but for a negative sign at \vec{g} .

Expression for ε_b becomes

$$\begin{aligned} \varepsilon_b &= (u_{b,j} + \vec{g}_j \cdot \vec{u}_j - u_{b,i} + \vec{g}_i \cdot \vec{u}_i) / l_{i,j} \\ &= (u_{b,j} + \{g_j\}^T \begin{Bmatrix} u_{t,j} \\ v_j \end{Bmatrix}) - u_{b,i} \\ &\quad + \{g_i\}^T \begin{Bmatrix} u_{t,i} \\ v_i \end{Bmatrix} / l_{i,j} \end{aligned} \quad (6)$$

where indices i and j denote the nodes of the element with the element local x axis from i to j . In the wake of it, the geometric matrix is modified to

$$[B] = \frac{1}{l} \begin{bmatrix} -1 & 0 & 0 & 1 & 0 & 0 \\ g_{i,x} & g_{i,y} & -1 & g_{j,x} & g_{j,y} & 1 \\ \lambda & -1 & -\lambda & \lambda & 1 & -\lambda \end{bmatrix} \quad (7)$$

with $\lambda = l/d/2$ and subscripts x and y indicating components of the vectors \vec{g} in the global coordinate system.

Different element lengths have to be used in the geometric Equation 7 and the volume integration implicit in 8. The top face nodes distance l is used in the former case, the reduced length $l_{red} = lR_{ax}/R_t = l r_{ratio}$ is used in the latter case. R_{ax} denotes the radius of the arch central axis, R_t is the radius of the top face curve. The element stiffness matrix for an arch element is

$$[K]_e = Ebd l_{red} [B]^T [D_{cs}] [B] \quad (8)$$

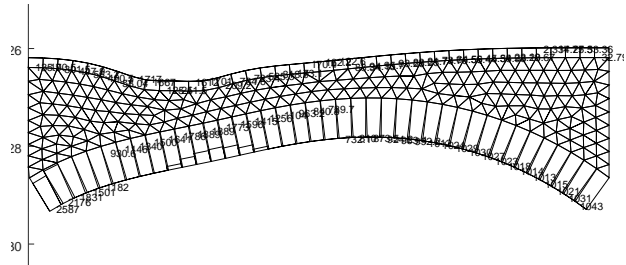


FIGURE 5. Bridge at Ponikla, compression stresses [kPa] and depths of the cracks in the bed joints

3. APPLICATION TO AN ARCH BRIDGE

Exclusive translational DOFs facilitate the combination of the TT element with simple 2D continuum elements. A dedicated matlab/octave code has been written to utilize this combination for the analysis of masonry arch bridges. The code features the simplest possible way how the interaction of the masonry arch, backfill and pavement can be assessed parallel with the principal pattern of failure of the masonry arch. The arch and pavement are modelled by the TT elements, the backfill by the classic constant strain triangle (CST) elements. Meshing of the backfill provides the Persson and Strang mesh generator, [8]. The no-tension cross-section model defined in Section 2.1 supports the cracking of the arch bed joints, which is the dominant pattern of the masonry arch bridge failure. The code includes a simple, purely vector graphics output. It consists of 1150 octave command lines, not including the mesh generator.

An application to the sandstone arch bridge at Ponikla in north Bohemia illustrates the code output in Figure 5. The span of the arch is 11.4 m. Two principal quantities are shown in each arch element, the maximum compression normal stress value inserted at the arch face where it occurs and the depth of the cracks in the bed joint. The load case is the design dead load combined with the tandem axle live loads with twice the design intensity level, i.e., 360 kN per wheel in lane 1 according to EN 1991-2.

The TT element and the masonry arch FEM models based on it claim to be the simplest models available to assess the most frequent failure mode of the stone masonry arches and the interaction of the arch with backfill and pavement.

4. 3D MINDLIN SHELL ELEMENT TM

The 2D models are often not adequate for the solution of masonry arches whose widths are mostly comparable to spans which makes the transverse variation of stresses and displacements nonuniform. A 3D analogue to the 2D TT element is, therefore, derived. The Mindlin assumptions, [9], and the simplest triangular facet shape are adopted, see Figure 6. The element local coordinate system features z axis normal to the facet plane. There is always a preference direction in the facet plane, the direction closest to the normals

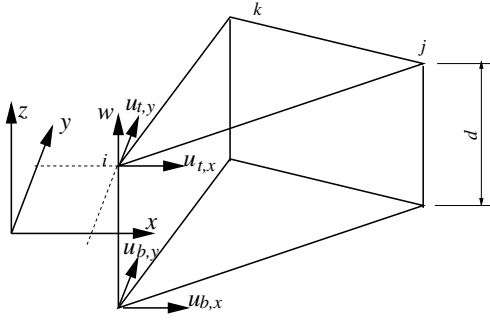


FIGURE 6. Geometry of the shell facet triangle element, the element local coordinate system and the DOFs at node i

to the bed joints planes of the masonry arch. It is assumed forthwith that the arch is a cylindric segment shell and the bed joints normals are tangents to the directrix of the cylinder so that their directions lie in a single plane. The global x axis is assumed to lie in that plane, too. In terms of the bridge nomenclature, the global x axis is in the direction of the arch span. The element local x axis is chosen as the direction closest to the global x within the element plane. The no-tension condition is applied to the σ_x (local x) normal stress component. Other options are possible and can be rather easily implemented in the code. It may be necessary in case of other than cylindric shells or more general failure modes and constitutive equations. Local y axis completes the element local right-handed cartesian coordinate system. All components are in this system up to Section 4.4, where two other systems are necessary.

Five translational DOFs per node are shown in Figure 6 for node i . They are ordered in matrix $\{u\}$ at each node, with node index omitted:

$$\{u\}^T = \{u_{t,x}, u_{t,y}, w, u_{b,x}, u_{b,y}\}$$

Deflection w and in-plane displacement vector \vec{u} are approximated by linear independent functions of natural triangular coordinates ξ_i .

$$w = \sum_i w_i \xi_i, \quad \vec{u} = \sum_i \vec{u}_i \xi_i$$

In literature, a common term for this kind of approximation is isoparametric element, not to be confused with true isoparametric elements for 2D and 3D continua. Derivatives of ξ_i are constants in the element area,

$$\frac{\partial \xi_i}{\partial x} = \frac{b_i}{2A}, \quad \frac{\partial \xi_i}{\partial y} = \frac{a_i}{2A} \quad \text{or} \quad \frac{\partial \xi_i}{\partial \vec{x}} = -\vec{n}_i \frac{l_i}{2A},$$

where A is the element area (note that $l_i/2A$ is the slope of the ξ_i surface upon the element area) and

$$\vec{n}_i = -\frac{1}{l_i} \begin{Bmatrix} b_i \\ a_i \end{Bmatrix}.$$

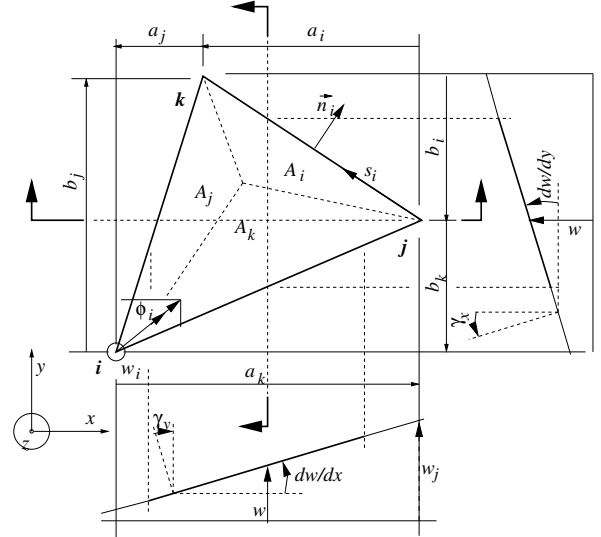


FIGURE 7. Triangular coordinates and shear deformation owing to deflection alone

Chain differentiation yields then

$$\gamma_{w,x} = -\frac{1}{2A} \sum_i w_i a_i, \quad \gamma_{w,y} = \frac{1}{2A} \sum_i w_i b_i \quad (9)$$

The shear deformation $\vec{\gamma}_w$ owing to deflection alone is

$$\gamma_{w,x} = -\frac{\partial w}{\partial y}, \quad \gamma_{w,y} = \frac{\partial w}{\partial x}, \quad (10)$$

note that *positive sense* is indicated in the figure for each of the four rotations and $\vec{\gamma}$ is the rotation of the normal to the element plane embedded in the material before deformation towards the normal to the element plane after deformation with standard sign convention of its components. In particular, the motion (rotation) shown in the section view right to left in Figure 7 goes from the inclined dashed line to the horizontal and γ_x is thus negative.

As in the TT element, the bending and shear deformation, are treated separately.

4.1. BENDING AND IN-PLANE DEFORMATION

Pseudocurvatures define the bending deformation. They are the derivatives of rotations of the normals to the element plane. The rotations of the normals in their turn depend on the in-plane displacements \vec{u} of the top and bottom faces of the element.

The element in-plane strains are specified in terms of the top and bottom faces (extrados and intrados) strain matrices $\{\varepsilon_t\}$ and $\{\varepsilon_b\}$ in analogy to the top and bottom uniaxial strains ε_t and ε_b in the Timoshenko 2D beam element. The element triangle geometry is defined in terms of distances $a_i = x_k - x_j$, $b_i = y_j - y_k$, where indices i, j, k are subjected to cyclic permutation and x_i, y_i specify node's i positions in the local system, see Figure 7. The geometric equations

of the CST triangle applied to the top face read

$$\begin{aligned} \{\varepsilon_t\} &= \begin{Bmatrix} \varepsilon_{t,x} \\ \varepsilon_{t,y} \\ 2\varepsilon_{t/b,xy} \end{Bmatrix} \\ &= \frac{1}{2A} \sum_i \begin{bmatrix} b_i & 0 \\ 0 & a_i \\ a_i & b_i \end{bmatrix} \begin{Bmatrix} u_{i,t,x} \\ u_{i,t,y} \end{Bmatrix}, \end{aligned} \quad (11)$$

substitute b for t subscript to get the bottom face strain matrix. The in-plane strains vary linearly across the element depth d ,

$$\{\varepsilon\} = z_t \{\varepsilon_t\} + z_b \{\varepsilon_b\} \quad (12)$$

where $z_t = (d + z)/d = 1 + \zeta$ and $z_b = -z/d = -\zeta$ are linear shape functions of the element in terms of the element local $0 > z > -d$ coordinate with $z = 0$ at the top face of the element or of the relative dimensionless $0 > \zeta > -1$ coordinate.

Plain stress conditions with $\sigma_{zz} = 0$ are assumed in the shell, then, the material stiffness matrix is

$$[D] = \frac{E}{1-\nu^2} \begin{bmatrix} 1 & \nu & 0 \\ & 1 & 0 \\ & & \frac{1-\nu}{2} \end{bmatrix} \quad (13)$$

for a linear elastic isotropic material. When cracked bed joints occur in planes normal to element's x axis, the conditions become vague. Adjacent to the cracked joints an approximately uniaxial stress prevails. It is thus assumed forthwith that the material stiffness matrix in the cracked elements is

$$[D(\{\varepsilon\})] = E \begin{bmatrix} s(\varepsilon_x) & 0 & 0 \\ & 1 & 0 \\ & & \frac{1-\nu}{2} \end{bmatrix} \quad (14)$$

where $s()$ is the normalized bilinear stress/strain diagram in the left sketch of Figure 2. It is obvious that the element local x axis must approximately coincide with the normals to the bed joints of the arch barrel.

The virtual work equation for cracked elements

$$\begin{aligned} \delta w &= \sum_i (\delta\{u_{i,t}\})^T \{g_{i,t}\} + \delta\{u_{i,b}\})^T \{g_{i,b}\} \\ &= \int_V \delta\{\varepsilon\}^T [D(\{\varepsilon\})] \{\varepsilon\} dV \\ &= E \int_V (\delta\varepsilon_x s(\varepsilon_x) + \delta\varepsilon_y \varepsilon_y + (1-\nu)\delta\varepsilon_{xy} \varepsilon_{xy}) dV \end{aligned} \quad (15)$$

delivers the expressions for the nodal forces $\{g_{i,t}\}$, $\{g_{i,b}\}$ when strains are expanded in terms of the virtual nodal displacements using Equation 11.

Functions $s_t(\varepsilon_{t,x}, \varepsilon_{b,x})$ and $s_b()$, see 2 in Section 2.1, return dimensionless top and bottom cross-section forces conjugate to top and bottom strains (input parameters) of a unit depth cross-section with $E = 1$ and no-tension stress-strain diagram. With the aid of the functions, the integrals in the virtual work

expression can be expressed in a closed form:

$$\begin{aligned} \delta w &= \frac{Ed}{2} (\delta\varepsilon_{t,x} s_t + \delta\varepsilon_{b,x} s_b + \delta\varepsilon_{t,y} (\varepsilon_{t,y}/3 + \varepsilon_{b,y}/6) \\ &+ \delta\varepsilon_{b,y} (\varepsilon_{t,y}/6 + \varepsilon_{b,y}/3) + (\delta\varepsilon_{t,xy} (\varepsilon_{t,xy}/3 + \varepsilon_{b,xy}/6) \\ &+ \delta\varepsilon_{b,xy} (\varepsilon_{t,xy}/6 + \varepsilon_{b,xy}/3)) (1-\nu)) \end{aligned} \quad (16)$$

Substitution by 11 and selection of individual nonzero virtual nodal displacements yields the expressions for the element nodal forces:

$$\begin{aligned} g_{i,t,x} &= \frac{Ed}{2} (b_i s_t + a_i (\varepsilon_{t,xy}/3 + \varepsilon_{b,xy}/6) (1-\nu)) \\ g_{i,t,y} &= \frac{Ed}{2} (a_i (\varepsilon_{t,y}/3 + \varepsilon_{b,y}/6) + \\ &+ b_i (\varepsilon_{t,xy}/3 + \varepsilon_{b,xy}/6) (1-\nu)) \\ g_{i,b,x} &= \frac{Ed}{2} (b_i s_b + a_i (\varepsilon_{t,xy}/6 + \varepsilon_{b,xy}/3) (1-\nu)) \\ g_{i,b,y} &= \frac{Ed}{2} (a_i (\varepsilon_{t,y}/6 + \varepsilon_{b,y}/3) + \\ &+ b_i (\varepsilon_{t,xy}/6 + \varepsilon_{b,xy}/3) (1-\nu)) \end{aligned} \quad (17)$$

Derivatives of the nodal forces $g_{i,t/b,x/y}$ with respect to the DOFs can be written in terms of the $s_{t/b}$ functions, for instance

$$\begin{aligned} \frac{\partial g_{i,t,x}}{\partial u_{j,t,x}} &= \frac{\partial g_{i,t,x}}{\partial \varepsilon_{t,x}} \frac{\partial \varepsilon_{t,x}}{\partial u_{j,t,x}} + \frac{\partial g_{i,t,x}}{\partial \varepsilon_{t,xy}} \frac{\partial \varepsilon_{t,xy}}{\partial u_{j,t,x}} \\ &= \frac{Ed}{4A} (b_i b_j \frac{\partial s_t}{\partial \varepsilon_{t,x}} + a_i a_j \frac{1-\nu}{2} \frac{1}{3}) \end{aligned}$$

Functions s_t , s_b depend on x components of ε_t , ε_b only. The subscript x can thus be omitted in their derivatives. Formulas for the derivatives are in Section 2.1. When $\mu = \frac{1-\nu}{2}$ is introduced and common factor $\frac{Ed}{4A}$ is omitted for brevity, submatrices $[K_{bend,i,j}]$ of the element stiffness matrix associated with the in-plane DOFs

$$\{u_{plane}\}^T = \{u_{i,t,x}, u_{i,t,y}, u_{i,b,x}, u_{i,b,y}\}$$

are:

$$\begin{aligned} i, i : & \begin{bmatrix} b_i b_j \frac{\partial s_t}{\partial \varepsilon_t} + a_i a_j \mu / 3 & a_i b_j \mu / 3 \\ a_j b_i \mu / 3 & b_i b_j \mu / 3 + a_i a_j / 3 \end{bmatrix} \\ i, j : & \begin{bmatrix} b_i b_j \frac{\partial s_t}{\partial \varepsilon_t} + a_i a_j \mu / 6 & a_i b_j \mu / 6 \\ a_j b_i \mu / 6 & b_i b_j \mu / 6 + a_i a_j / 6 \end{bmatrix} \\ j, i : & \begin{bmatrix} b_i b_j \frac{\partial s_b}{\partial \varepsilon_b} + a_i a_j \mu / 6 & a_i b_j \mu / 6 \\ a_j b_i \mu / 6 & b_i b_j \mu / 6 + a_i a_j / 6 \end{bmatrix} \\ j, j : & \begin{bmatrix} b_i b_j \frac{\partial s_b}{\partial \varepsilon_b} + a_i a_j \mu / 3 & a_i b_j \mu / 3 \\ a_j b_i \mu / 3 & b_i b_j \mu / 3 + a_i a_j / 3 \end{bmatrix} \end{aligned} \quad (18)$$

For a linear element (uncracked bed joints) $[K_{i,j}]^T = [K_{j,i}]$, which implies symmetry of the whole matrix $[K]$. For cracked bed joints $h_{t,b} \neq h_{b,t}$, the symmetry is lost.

4.2. SHEAR OWING TO THE ROTATIONS OF NORMALS

The rotation of normals $\vec{\varphi}$ induces shear deformation, too. It would not induce any deflection in a consistent isoparametric element and then $\vec{\varphi}$ would simply be added to $\vec{\gamma}$ to obtain the total shear deformation. Such displacement pattern is known to imply locking in thin elements, like it does in the isoparametric variant of the TT element. In the TM element, $\vec{\varphi}$ induces a quadratic field of deflection w_φ , which must have zero values at all joints. The deflection should be compatible with the neighbouring elements along the boundaries. The antisymmetric part of the normal component of $\vec{\varphi}$ along an element's side is assigned to deflection, the symmetric part to shear deformation, in analogue, to the TT element. Perfect compatibility of deflections along boundaries with neighbouring elements is attained for elements lying in a plane. The implementation of the outlined displacement pattern is rather lengthy and it is skipped here. The resulting constant transverse shear owing to normals rotation is

$$\gamma_u = \sum_i [\psi_i] (\{u_{i,t}\} - \{u_{i,b}\})$$

$$[\psi_i] = \left(\begin{bmatrix} 0 & -1/3 \\ 1/3 & 0 \end{bmatrix} - \frac{1}{12A} \begin{bmatrix} a_k^2 - a_j^2 & b_j a_j - b_k a_k \\ -b_k a_k + b_j a_j & b_j^2 - b_k^2 \end{bmatrix} \right) \frac{1}{d} \quad (19)$$

The full transverse shear of the TM element is then

$$\{\gamma\} = \sum_i \left([\psi_i], \frac{1}{2A} \begin{bmatrix} -a_i \\ b_i \end{bmatrix}, -[\psi_i] \right) \{u\}_i \quad (20)$$

where indices i, j, k are subject to cyclic replacement. Formula 20 is necessary with thin shells where shear locking can occur. Masonry arches and other burried shells are mostly thick shells. Matrices $[\psi_i]$ can be simplified by omitting the second summand in such applications. Experience with tests and applications testifies that keeping the second summand improves the element convergence.

4.3. TM FLAT SLAB ELEMENT

Simple linear constitutive equations are assumed for the transverse shear,

$$V_x = G\gamma_x, \quad V_y = G\gamma_y. \quad (21)$$

V_x is the standard shear force in element local $y - z$ plane when looking along x axis and V_y is the standard shear force in element local $x - z$ plane when looking along y axis.

The contribution of the shear stiffness to the element stiffness matrix is written down in terms of the 5x5 submatrices associated with the two top vertex, one transverse and two bottom vertices translational DOFs of each node. Column matrices $[\varphi_i] = [-a_i, b_i]^T / 2A$

and 2x2 symmetric matrices $\psi_{ij} = [\psi_i]^T [\psi_j]$ help to write down the shear contribution to the submatrices:

$$[K_{shear,i,j}] =$$

$$GA d^2 \begin{bmatrix} [\psi_{ij}] & [\psi_i]^T [\varphi_j] & -[\psi_{ij}] \\ [\varphi_i]^T [\psi_j] & [\varphi_i]^T [\varphi_j] & -[\varphi_i]^T [\psi_j] \\ -[\psi_{ij}] & -[\psi_i]^T [\varphi_j] & [\psi_{ij}] \end{bmatrix} \quad (22)$$

Complete 5x5 stiffness submatrices are the sums of the bending stiffness submatrices 18 extended by an empty third column and row inserted between the 2x2 subsubmatrices and submatrices 22:

$$[K_{i,j}] = [K_{bend,i,j}]_{extended} + [K_{shear,i,j}] \quad (23)$$

The whole element stiffness matrix is the size 15x15 composition of submatrices $[K_{i,j}]$, but the submatrices are assembled in the global stiffness matrix so that the whole matrix is never set up.

Cracking in the bed joints followed by development of virtual hinges in the arch have been considered the dominant failure pattern of masonry bridges since the early attempts [10], [11] to assess the load capacity. Other failure modes like shear sliding of the bed joints or transverse tension cracking of the arch require sophisticated material models and properties which are almost impossible to obtain in the design practice.

This stiffness matrix can be used for the solution of flat slabs loaded both in and out of plane but in shells, the bottom face DOFs $u_{b,x}$, $u_{b,y}$ require a special treatment since they are not simply shared by the elements attached to a node.

4.4. TM SHELL ELEMENT

The DOFs at the bottom vertices of the elements connecting to a node do not lie in the same plane and are not independent of the DOFs at the top vertices. The equilibrium of the nodal forces at the top vertices is affected by the nodal forces at the bottom vertices. These two conjugate deficiencies must be removed.

The normal to the shell surface is needed for a consistent formulation of the TM element. The normal is rigid in the frame of the Timoshenko-Mindlin shell theory, which implies that the displacements of all points of the normal share the same lateral displacement component. The exact definition of the normal direction \vec{n} would be through the shell surface mathematical definition. For practical applications of the TM element, it is sufficient to define the unit normal \vec{n}_i at a node i as the normalized sum of the normals of all elements connecting to the node, each element normal length proportional to the sine of the angle of the two adjacent sides of the respective element. Position vectors of nodes are denoted \vec{x}_i and nodes of the connecting elements i, j, k , ordered counterclockwise when viewed from the top side of the shell. The sum is

$$\vec{n}_{s,i} = \sum_e \vec{n}_e \sin(\alpha_e) =$$

$$\sum_e (\vec{x}_j - \vec{x}_i) \times (\vec{x}_k - \vec{x}_i) / (|\vec{x}_j - \vec{x}_i| |\vec{x}_k - \vec{x}_i|)_e$$

$$\vec{n}_i = \vec{n}_{s,i} / |\vec{n}_{s,i}|$$

Vector \vec{n}_i 's positive direction is outwards from top surface of the shell. The vector also defines the tangential plane τ_i at node i , $\tau_i \perp \vec{n}_i$. The top vertices of the connecting elements share the displacement $\vec{r}_{t,i}$ of the top end of the rigid normal. The global components of vector $\vec{r}_{t,i}$ constitute the first three DOFs of the node i . The index of the node is omitted forthwith since a single node is considered.

The compatibility of displacements at the bottom facets of the connecting elements demands that the projections on the τ plane of the bottom vertices displacements of all connecting elements share the same displacement vector $\vec{r}_{b,\tau} \subset \tau$. A coordinate system is established in the τ plane such that axis 1 direction vector \vec{n}_1 lies in the intersection of the global coordinates plane $x-z$ and the τ plane, oriented as the global x axis. Axis 2 direction vector is $\vec{n}_2 = \vec{n} \times \vec{n}_1$ (vector product). The component expansion of vector $\vec{r}_{b,\tau}$ is defined this way. The two components in the τ plane define the two complementary DOFs of the node. Note that they are not the displacement components in the global coordinate system $x-y-z$ but in the local 'tangential' plane instead.

The transformation matrix from global to these tangential vector components is

$$[T]_\tau = \begin{bmatrix} \{n_1\}^T \\ \{n_2\}^T \\ \{n\}^T \end{bmatrix} \quad (24)$$

The whole bottom vertices displacement vector is

$$\vec{r}_b = \vec{r}_{b,\tau} + \vec{n}(\vec{n} \cdot \vec{r}_t) = \vec{r}_{b,\tau} + \vec{n} \otimes \vec{n} \vec{r}_t,$$

but just the two components of $\vec{r}_{b,\tau} \subset \tau$ constitute the two complementary DOFs of the node. The out-of- τ -plane component depends on the basic three DOFs \vec{r}_t of the node. Several coordinate systems (all cartesian) are employed. The global one, common for all, the τ system, common for a node and the local e systems of individual elements. *The convention is adopted for component matrices that the matrix with components in the global system has no subscript τ , in the τ system, and subscripts e in the element systems.* Furthermore, the transformation matrix $[T]_e$ from the global to the element system has subscript e . The matrix form of the expression for the element DOFs is

$$\begin{Bmatrix} \{r_t\}_e \\ \{r_b\}_e \end{Bmatrix} = \begin{bmatrix} [T]_e & 0 \\ [T]_e \{n\} \{n\}^T & [T]_e [T]_\tau^T \end{bmatrix} \begin{Bmatrix} \{r_t\} \\ \{r_b\}_\tau \end{Bmatrix} \quad (25)$$

Recall that both the displacement component matrices $\{r_b\}_e$ and $\{r_b\}_\tau$ have zero third components so that the third column and row of the transformation matrix in 25 can be omitted.

The nodal forces conjugate to $\{r_t\}_e$ and $\{r_b\}_e$ are denoted $\{g_t\}_e$ and $\{g_b\}_e$. Rigid normals to the shell surface imply that the equilibrium equations of the

top and bottom joints of a node are not independent. Just a single equilibrium equation can be written in the direction \vec{n} and it is assigned to the top end of the rigid normal – the top joint of the node. The two remaining equations at the bottom joint of the node include components acting in the τ plane. Component decompositions of the element nodal forces in the coordinate axes tripod $\vec{n}_1, \vec{n}_2, \vec{n}$ – the node local τ system, are added in the matrix equilibrium equation of the bottom joint of the node:

$$\sum_e \{g_b\}_{\tau,e} = \sum_e [T]_\tau [T]_e^T \{g_b\}_e = \begin{Bmatrix} 0 \\ 0 \\ \{n\} \{n\}^T \{g_b\}_e \end{Bmatrix}$$

The sum includes all elements connecting at the node. The third (transverse) components are added to forces acting at the top vertex of the node to obtain the final nodal forces of the element:

$$\begin{Bmatrix} \{g_t\} \\ \{g_b\}_\tau \end{Bmatrix} = \sum_e \begin{bmatrix} [T]_e^T & \{n\} \{n\}^T [T]_e^T \\ 0 & [T]_\tau [T]_e^T \end{bmatrix} \begin{Bmatrix} \{g_t\}_e \\ \{g_b\}_e \end{Bmatrix} \quad (26)$$

The transformation matrices of the nodal displacements and forces are transpose of each other, which testifies to their correctness.

Note that the last scalar equations in 25 and 26 can be omitted and so can be the last columns of the transformation matrices. The transformation matrices are then 5×5 in size. They are specific for each node of an element since the $\{n\}$ and $[T]_\tau$ matrices are different at each node. For an easy reference, they are denoted $[T_i]$ for node i forthwith. The submatrices $[K_{i,j}]$ are transformed to the global coordinate system

$$[K_{i,j}]_g = [T_i]^T [K_{i,j}] [T_j] \quad (27)$$

and assembled in the system matrix.

4.5. TM ELEMENT CODE AND TEST

The TM element has been implemented in a dedicated Matlab/Octave code including a simple graphic output. Just the shell reference surface is drawn to keep the view readable. The maximum compression stresses in the bed joints and the relative depth of the cracks are inserted in each element. These values are sufficient to decide on the arch load capacity in the context of the present model. The graphic output uses vector graphics so that pictures can be zoomed in with a stable resolution. The mesh generator [8] is used for the shell surface meshing. The code is entirely self-contained, no input data file and pre- or postprocessing is necessary. It contains just about 660 octave command lines, not including the mesh generator.

The pinched cylinder with rigid end diaphragms in Figure 8 is a popular benchmark to test shell elements. The shell is thin, $d/R = 0.01$ so that the test is a severe one for a thick shell element. The benchmark solution by double Fourier series with 80 terms in both directions was first presented in [12] based on

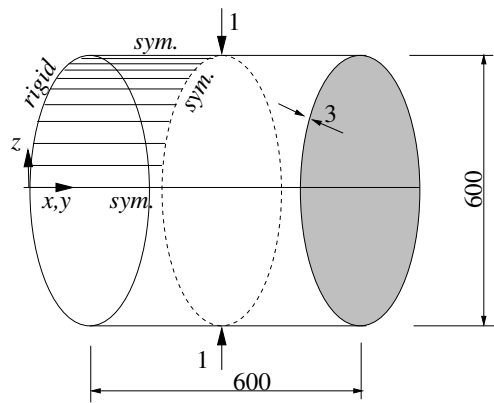


FIGURE 8. Benchmark shell

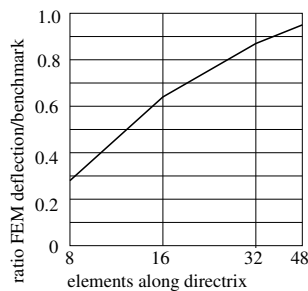


FIGURE 9. Convergence of the FEM deflections, ratio to the benchmark deflection

the work [13]. The Kirchhoff-Love kinematic assumptions are used in the benchmark so that a definite deflection is obtained. Differences can be expected between the present and benchmark solutions in the vicinity of the pin force, in particular for fine meshes. The Mindlin assumptions imply infinite deflection beneath the force in the continuum model, thus making the discretized models mesh dependent and inherently non-convergent. Owing to the three symmetry planes just shaded, $1/8$ of the cylinder can be considered. Four mesh densities were considered with 8, 16, 32 and 48 elements along the directrix. The ratio of the loaded node deflection of the TM finite element solutions to the benchmark deflection $1.825 \cdot 10^{-5}$ is shown in Figure 9. In spite of the correction of the transverse shear strain in Equation 20, the residual shear locking still persisted and affected the results in this thin shell, in particular, for low density meshes. In order to reduce it further, the material shear stiffness in the transverse direction (element local $x-z$ and $y-z$ planes) was selectively lowered eight times. This has a negligible effect on the overall response of the FEM model since the contribution of the transverse shear compliance to it is small. At the denser mesh side of the Figure 9, the curve already tends to adopt to the infinite deflection of the continuum Mindlin shell and break the Kirchhoff-Love benchmark limit. The deformed mesh is shown in Figure 10. The radial component of the deflection along the directrix from the benchmark solution [12] in Figure 11 compares well to the deformed mesh in Figure 10, note

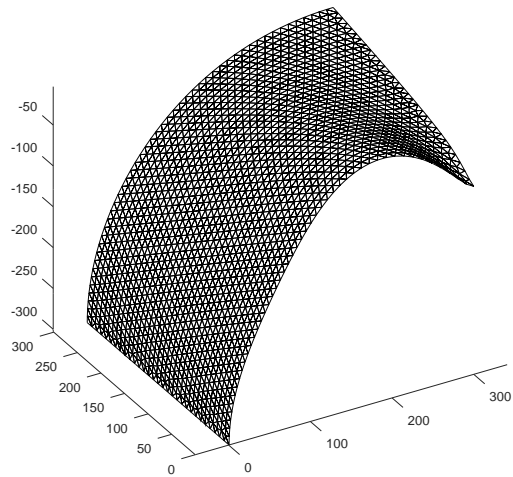


FIGURE 10. Deformed mesh, 48 elements along the directrix

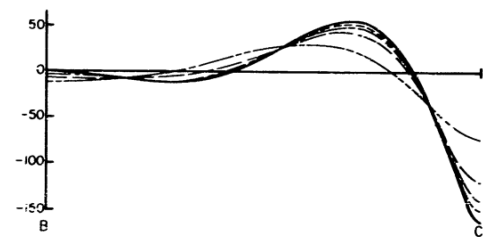


FIGURE 11. Radial component of deflection along the directrix, benchmark by the solid line, [12]

the shallow inward deflection in the lower part of the front directrix. The precision and convergence of the deflection beneath the pin force is, as expected, worse than for elements based on the Kirchhoff-Love assumptions.

A solution of the Ponikla bridge arch loaded by characteristic arch selfweight and standard LM1 tandem axle with wheel forces of 250 kN is provided for the illustration of the code output in Figure 12. Displacements are 2000 times scaled up. In comparison to the 2D solution of the same bridge arch in Section 3, the interaction and selfweight of the fill and pavement are not accounted for, the tandem axle load and mesh density are slightly different, too. The tandem axle position in the transverse direction is the extreme eccentric one within the bounds defined by the EN 1991-2. The differences between the loaded/unloaded sides of the arch barrel are 1261/405 kPa in extreme normal stresses in the bed joints and 0.41/0.25 in relative crack depths. The backfill and pavement stiffness and selfweight reduce the differences in the real bridge, but the example testifies that the 2D models need corrections. The 3D bridge model analogue to the one in Section 3 is currently being worked on.

The absence of rotational DOFs improves the convergence of the iterations. The no-tension, history independent material model admits a single load increment strategy. In the illustration example, the

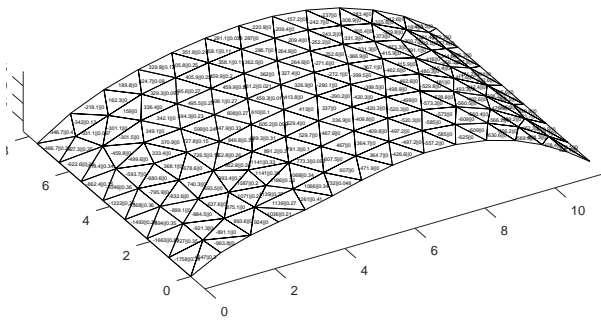


FIGURE 12. Bridge at Ponikla, 3D shell, compression stresses [kPa] and relative depths of the cracks in the bed joints

ratio 0.005 of the RMS norms of the imbalance and load was reached in 3 iterations.

5. CONCLUSIONS

The simplest finite elements for 2D and 3D thick shells have been developed for applications in masonry arch bridges limit load analysis. They feature seamless combination with 2D CST and 3D tetrahedron elements for the bridge's backfill. Exclusively translational DOFs are used, which improves the convergence of iterations. The no-tension condition is applied to the normal stress in the bed joints planes. The output minimum normal stresses and cracks depths in these planes can be used to assess the ultimate limit loads of a bridge. A sample analysis of an arch of the bridge at Poniklá testifies that this material law and shell elements develop a characteristic failure mode of the stone masonry arch bridges, the gradual creation of the virtual hinges.

ACKNOWLEDGEMENTS

The author was supported by the grant NAKI DG20P02OVV001, 'Tools for the preservation of historical values and functions of arch and vaulted bridges' provided by the Ministry of Culture of the Czech Republic.

REFERENCES

- [1] The Highways Agency, London. *Design manual for roads and bridges, vol. 3, Highway structures: inspection and maintenance, section 4, Assessment, Part 3, The assessment of highway bridges and structures*, 2001.
- [2] Ministry of transport of the Czech Republic. *Zatížitelnost zděných klenbových mostů - Load rating of masonry arch bridges*, 2008.
- [3] T. E. Ford, C. E. Augarde, S. S. Tuxford. Modelling masonry arch bridges using commercial finite element software. In *Proceeding of the 9th International Conference on Civil and Structural Engineering Computing*. Civil-Comp Press, Stirling, 2001.
- [4] Mott-MacDonald, 20-26 Wellesley road, Croydon, CR9 2UL, UK. *CTAP manual for the assessment of masonry arch bridges*, 1990.
- [5] R. Bridle, T. Hughes. An energy method for arch bridge analysis. *Proceedings of the Institution of Civil Engineers* **89**:375–385, 1990. <https://doi.org/10.1680/iicep.1990.9397>.
- [6] M. Gilbert. RING: a 2D rigid block analysis program for masonry arch bridges. In *Proceedings of the 3rd International Arch Bridges Conference*, pp. 459–464. 2001.
- [7] W. Harvey. Application of the mechanism analysis to masonry arches. *Structural engineer* **66**:77–84, 1988.
- [8] P.-O. Persson, G. Strang. Simple mesh generator in MATLAB. *SIAM Review* **46**(2):329–345. <https://doi.org/10.1137/S0036144503429121>.
- [9] R. D. Mindlin. Influence of rotatory inertia and shear on flexural motions of isotropic, elastic plates. *ASME Journal of Applied Mechanics* **18**(1):31–38, 1951. <https://doi.org/10.1115/1.4010217>.
- [10] A. Pipard, R. Ashby. An experimental study of a voussoir arch. *Proceedings of the Institution of Civil Engineers* **10**:383, 1938.
- [11] A. J. S. Pippard. *The civil engineer in war*, vol. 1, chap. The Approximate Estimation of Safe Loads on Masonry Bridges., pp. 365–372. 1948. <https://doi.org/10.1680/ciww1.45170.0021>.
- [12] G. Lindberg, M. D. Olson, G. R. Cowper. New developments in the finite element analysis of shells, 1969. <https://apps.dtic.mil/sti/pdfs/AD0707780.pdf>.
- [13] W. Flugge. *Stresses in shells*. Springer Verlag, 1962.